Algorithm Controlling the Autonomous Flight of an Unmanned Aerial Vehicle Based on the Construction of a Glider

Lucjan Setlak and Rafał Kowalik
Aviation Division, Department of Avionics and Control Systems
Polish Air Force University
Deblin 08-521, ul. Dywizjonu 303 No. 35
Poland
l.setlak@law.mil.pl, r.kowalik@law.mil.pl

Abstract: - This article is devoted to the objects of unmanned aircrafts as well as their flight control systems in particular. Their analysis in the light of the critical analysis of the literature on the subject of research includes the characteristics of unmanned objects based on the construction of a glider, discussion of their applications in the context of various configurations depending on the purpose and type of mission. The main goal of the work is to develop an algorithm for controlling the autonomous control system of a UAV object, based on a mathematical model that describes the unmanned aircraft mechanics with small dimensions using a mathematical apparatus. Additionally, for the purpose of the analysis, general subsystems included in unmanned aerial vehicles were listed and characterized. On the other hand, based on the created model of the flying object, an algorithm was developed to increase flight stability taking into account the turning maneuver. On the basis of the conducted research, the results obtained from simulation tests carried out in the Matalb/Simulink programming environment were presented. In the final part of the work, based on the considerations made at the beginning in the field of the subject of the research, the mathematical model created using mathematical analysis and the obtained research results, conclusions drawn in practical applications were drawn.

Key-Words: - Control algorithm, autonomous flight, unmanned aerial vehicle, glider, flight control systems, mathematical model, programming environment

1 Introduction

For the purpose of developing reconfiguration algorithms based on the use of the control allocation method, a small unmanned aerial vehicle was selected. It is characterized by the following basic technical parameters, i.e. an object with a wingspan of 2.6 [m], a total length of 1.25 [m], take-off mass up to 3 [kg] and the maximum thrust of the drive unit 10 [N]. In addition, the selected model was used to perform simulation tests of the developed algorithms [1], [2], [3], [4].

The aircraft was modeled as a rigid platform characterized by six degrees of freedom, and a disengaged control surface deflection system in which each of its control surfaces has the possibility of independent deflection [5], [6].

In addition, the following assumptions were made for the development of the dynamic unmanned aircraft (UAV) model [7]:

- invariance of mass parameters (mass, position of the center of gravity, moments of inertia) in flight;
- the cruising speed of the aircraft's movement is approximately 16 [m/s] at an altitude of up to 30 [m];
- the control surfaces of the object are deflected without delay.

In turn, the following right-hand Cartesian coordinate systems have been adopted for the spatial description of the aircraft's motion (Fig. 1):

- *inertial, Earth's coordinate system* $O_n x_n y_n z_n$- of the beginning at the O_n point located at any point on the Earth's surface, where the $O_n z_n$ axis is convergent with the direction of the Earth acceleration vector, the $O_n x_n y_n$ plane is tangent to the Earth's surface, the $O_n x_n$ axis is directed in the direction of North Geography , while the $O_n y_n$ axis is directed to the east;
- *gravity coordinate system* $O_g x_g y_g z_g$- referring to a moving object, the origin of the system O_g is located in the center of gravity of the aircraft, the system being parallel to the inertial system $O_n x_n y_n z_n$ and having equally directed axes;

$$T_V = \begin{bmatrix} \cos\Theta \cdot \cos\Psi & \sin\Theta \cdot \sin\Phi \cdot \cos\Psi - \cos\Phi \cdot \sin\Psi & \cos\Phi \cdot \sin\Theta \cdot \cos\Psi + \sin\Phi \cdot \sin\Psi \\ \cos\Theta \cdot \sin\Psi & \sin\Theta \cdot \sin\Phi \cdot \sin\Psi + \cos\Phi \cdot \cos\Psi & \cos\Phi \cdot \sin\Theta \cdot \sin\Psi - \sin\Phi \cdot \cos\Psi \\ -\sin\Theta & \sin\Phi \cdot \cos\Theta & \cos\Phi \cdot \cos\Theta \end{bmatrix} \quad (3)$$

– *the coordinate system* $O_bx_by_bz_b$- is the system associated with the aircraft, the beginning of the system O_b coincides with the beginning of the gravity system O_g, the axis O_bx_b is on the symmetry plane of the aircraft, the axis $O_bx_bz_b$ passes along the aircraft and is directed towards the front part of the hull, O_bz_b axis directed downwards in accordance with the direction of the aircraft's chassis, while the O_by_b axis complements the right-hand system and is directed to the right.

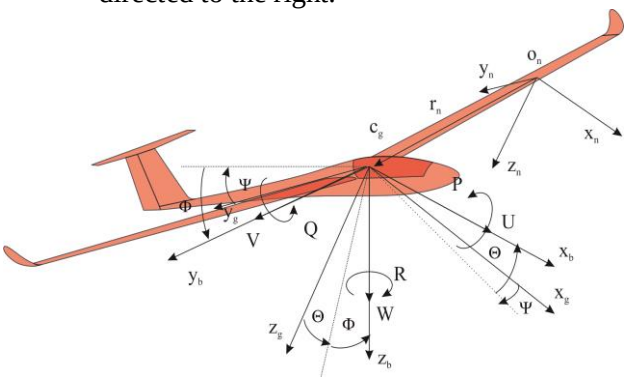

Fig. 1 Coordinate systems

The equations of motion of the aircraft were derived based on the coordinate system associated with the aircraft $O_bx_by_bz_b$. The aircraft state vector x contains linear velocity components $v = [U\ V\ W]$, where: U- longitudinal speed, V- transverse velocity, W- vertical velocity and angular velocity $\omega = [P\ Q\ R]$, where: P- angular velocity of tilt, Q- angular velocity of inclination, R- angular velocity of the deviation, which is illustrated in the figure above [8], [9], [10], [11].

In turn, the position and orientation of the aircraft is described by means of a vector with the coordinates $y = [x_n\ y_n\ z_n\ \varphi\ \Theta\ \Psi]^T$, where: x_n, y_n, z_n- are constituents of the vector r_n of the center of gravity position *(cg)* of the aircraft in the Earth's coordinate system $O_nx_ny_nz_n$, φ- is the angle of tilt, Θ- the angle of inclination and Ψ- the angle of deviation of the aircraft, as shown in the figure above [12], [13], [14], [15].

Relations between the state vector $x = [U\ V\ W\ P\ Q\ R]^T$ and the vector of the position y describe the following expressions [16], [17]:

$$\dot{y} = Tx \quad (1)$$

where: matrix T takes the form:

$$T = \begin{bmatrix} T_V & 0 \\ 0 & T_\Omega \end{bmatrix} \quad (2)$$

including:

$$T_\Omega = \begin{bmatrix} 1 & \sin\Phi \cdot \tan\Theta & \cos\Phi \cdot \tan\Theta \\ 0 & \cos\Phi & -\sin\Phi \\ 0 & \sin\Phi \cdot \sec\Theta & \cos\Phi \cdot \sec\Theta \end{bmatrix} \quad (4)$$

The general form of traffic equations describes the expression:

$$A\dot{x} + Bx = f_A + f_G + f_T \quad (5)$$

where: f_A- is the vector of the aerodynamic load, f_G- is the vector of the gravitational load, f_T- is the vector of the thrust.

$$B = \Omega \quad (6)$$

where matrices A and Ω have the forms:

$$A = \begin{bmatrix} m & 0 & 0 & 0 & 0 & 0 \\ 0 & m & 0 & 0 & 0 & 0 \\ 0 & 0 & m & 0 & 0 & 0 \\ 0 & 0 & 0 & I_x & 0 & -I_{xz} \\ 0 & 0 & 0 & 0 & I_y & 0 \\ 0 & 0 & 0 & -I_{xz} & 0 & I_z \end{bmatrix},$$

$$\Omega = \begin{bmatrix} 0 & -R & Q & 0 & 0 & 0 \\ R & 0 & -P & 0 & 0 & 0 \\ -Q & P & 0 & 0 & 0 & 0 \\ 0 & -W & V & 0 & -R & Q \\ W & 0 & -U & R & 0 & -P \\ -V & U & 0 & -Q & P & 0 \end{bmatrix} \quad (7)$$

where: m- is the mass of the aircraft, I_x, I_y, $Iż$- determine the moments of inertia, while I_{xz}- is the deviant moment of inertia.

The aerodynamic load vector takes the form [18]:

$$f_A(x, y, \delta) = [f_a(x, y, \delta] \quad m_a(x, y, \delta)]^T \quad (8)$$

The control vector contains the following elements:

$$\delta = [\delta_{AR} \quad \delta_{AL} \quad \delta_{ER} \quad \delta_{EL} \quad \delta_{FR} \quad \delta_{FL} \quad \delta_R]^T \quad (9)$$

where: δ_{AR}- right aileron deflection angle, δ_{AL}- left wing deflection angle, δ_{ER}- right rudder deflection angle, δ_{EL}- left rudder deflection angle, δ_{FR}- deflection angle of the right flap, δ_{FL}- deflection angle of the left flap, δ_R- deflection angle of the rudder.

Vectors of aerodynamic force and moment can be expressed as sums:

$$f_a = F_{AS} + F_{A\Omega} + F_{AW} + F_{A\delta} \quad (10)$$

$$m_a = M_{AS} + M_{A\Omega} + M_{AW} + M_{AV} + M_{A\delta} \quad (11)$$

where: F_{AS} and M_{AS}- are static aerodynamic and aerodynamic vector vectors that are derived from angle of attack, slip angle and Mach number, $F_{A\Omega}$ and $M_{A\Omega}$- are aerodynamic force and momentum vectors derived from linear velocity, M_{AV}- is a vector of aerodynamic moment derivative transverse

velocity, F_{AW} and M_{AW}- are aerodynamic force and moment vectors which are derivatives of vertical acceleration and $F_{A\delta}$ and $M_{A\delta}$, which are derivatives of angles of control surface tilts [19], [20].

2 Methods and Algorithms for Reconfiguration

The presented reconfiguration method was developed for a small unmanned aerial vehicle with a classic control system, consisting of one pair of ailerons, one pair of elevator, a pair of flaps and a single rudder.

In the adopted method of reconfiguration it is assumed that each control surface of the UAV object can be tilted independently, which means that the control system uses seven independent control surface mechanisms (Fig. 2).

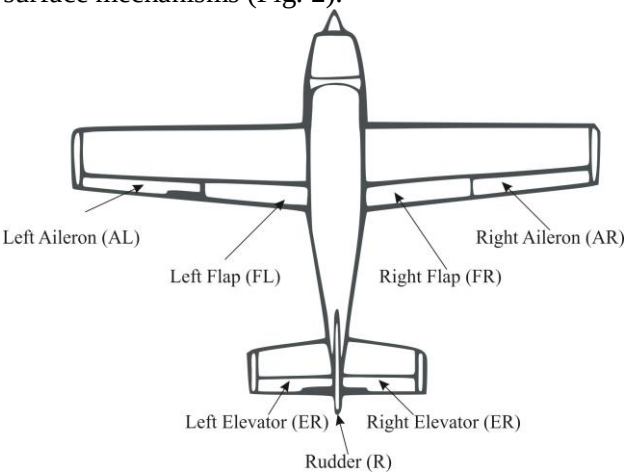

Fig. 2 Configuration of the UAV object control system

The developed reconfiguration method uses information received from control surfaces after detection of a control system failure and a model of aerodynamic loads produced by individual control surfaces. The method assumes that the fault is detected and identified and that all necessary variables of the flight conditions are measured [21], [22], [23], [24].

The general structure of the reconfiguration system is illustrated in the figure below (Fig. 3).

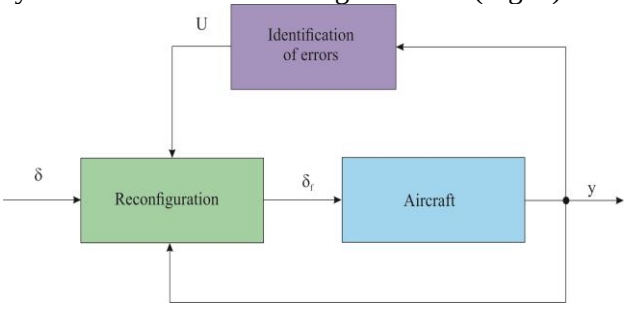

Fig. 3 General block diagram of the control system

The three-component vector $\delta = [\delta_{L0} \ \delta_{H0} \ \delta_{R0}]^T$ is provided as an input signal containing the values of the angle of aileron, rudder and rudder heights determined by the operator or by the automatic flight control system. The same control vector is given at the entrance in a failure-free condition.

In addition, the system receives information on which control surface is blocked and what is its current swing angle υ [25], [26], [27].

The reconfiguration algorithm calculates the angles of deflection of efficient rudder surfaces δ_f and creates a model of derivative that can be controlled. However, the quantities of deflections of efficient control devices are determined in such a way that the aerodynamic and aerodynamic torque vectors generated by the damaged and operating control cylinders are immutable, i.e. they have the same orientation, value and physical sense. The problem defined in this way can be solved in many ways [28], [29].

The article presents four different variants of the algorithm that implements this reconfiguration method. These variants differ in terms of the applied aerodynamic load models from control and in the formulation of comparable control load vectors and the applied optimization [30].

In the first variant of the reconfiguration algorithm (variant 1) a linear model of aerodynamic load was used. This model omits the component x of the aerodynamic force assuming that its effects will be compensated by the changed thrust train sequence.

The linear equation (5) describing the dynamics of the aircraft in a failure-free condition (hereinafter referred to as the reference model), with a limitation of five degrees of freedom (according to the abovementioned reference model assuming that the force acting along the x-axis is omitted) is [31]:

$$\dot{x}_m = A_m x_m + B_m \delta \tag{12}$$

where: δ- is the input control vector, generated by the operator or by the automatic control system.

According to the adopted assumptions, the reference model's state vector has the following form [32]:

$$x_m = [V \ \ W \ \ P \ \ Q \ \ R]^T \tag{13}$$

The model of the aircraft after the failure can be presented as follows:

$$\dot{x}_f = A_f x_f + B_f \delta_f + \upsilon \tag{14}$$

where: υ- is the vector of the disturbance state caused by the failure, x_f- is the state vector having the same components as the x_m vector, and δ_f - is the

vector covering the four angles of deflection of control surfaces, according to the formula (9).

The purpose of this reconfiguration algorithm is to provide the same response of a damaged aircraft to an input control signal, as in the case of a fully functional aircraft, namely [33]:

$$e = \dot{x}_m - \dot{x}_f = 0 \tag{15}$$

which implies the following reactions:

$$A_f x_f + B_f \delta_f + v = A_m x_m + B_m \delta \tag{16}$$

Assuming that the defects in the control systems have little effect on the dynamic characteristics of the aircraft, it can be assumed that:

$$A_f x_f \approx A_m x_m \tag{17}$$

therefore the condition described by equation (16) can be reduced to the following form:

$$B_f \delta_f + v = B_m \delta \tag{18}$$

Hence we get the formula for the vector control of the damaged aircraft:

$$\delta_f = B_f^{-1}(B_m \delta - v) \tag{19}$$

The above formula is an algebraic equation that does not take into account the physical limitations of the control system and which does not guarantee the determination of the optimal control vector δ_f.

The result obtained in this way is not always unambiguous, because the system of equations may not have solutions (i.e. they may be undefined) or the number of unknown variables may differ from the number of equations [34], [35].

In order to obtain a clear and optimal solution, the algorithm was modified using the optimization method to determine the control vector of the inefficient aircraft, while the optimization criterion was to minimize the angles of deflection of the control surfaces.

The problem formulated in this way allows to gain control over the damaged aircraft to an extent comparable to a fully functional aircraft and limits the possibility of deflecting control surfaces over acceptable angles, with the modified algorithm described as option 2.

As in the case of the previous algorithm, the control vector δ_f is searched for which the equation (18) is true. In this variant of the reconfiguration algorithm, this relationship is the equation of limitations of the optimization algorithm in the function, which is the sum of squares of the angles of deflection of working surfaces.

$$f_{\delta_f} = {\delta_{f,1}}^2 + {\delta_{f,2}}^2 + \cdots + {\delta_{f,i}}^2 + \cdots \tag{20}$$

The problem is to find such angles of deflection of control working surfaces for which the general function (20) is minimized and at the same time the equation of constraints (18) is satisfied:

$$\min_{\delta_f} f_{\delta_f} \; dla \; \{B_f \delta_f + v - B_m \delta = 0\} \tag{21}$$

The equation of constraints used in the second algorithm is a time-constant linear equation that does not refer to the control variables of the state vector derivative. Therefore, the response of the reference model will differ from the response of the actual aircraft.

Therefore, another algorithm was developed (variant 3), in which the equation of limits was formulated based on a non-linear model of aerodynamic loads induced by an input control signal (equations 10 and 11).

As in the previous algorithm (variant 2), the control surface deflections are set below the limits, and the function described by equation (20) is minimized.

Therefore, the problem of determining the minimum deflections of the steering gear can be expressed in the following way [36]:

$$\min_{\delta_f} f_{\delta_f} \; dla \; \{f_{A\delta}(x, y, \delta_f, v) - f_{A\delta}(x, y, \delta) = 0\} \tag{22}$$

where:

$$f_{A\delta}(x, y, \delta) = \left[F_{A\delta}^{y,z}(x, y, \delta) \quad M_{A\delta}(x, y, \delta\right]^T \tag{23}$$

$$f_{A\delta}(x, y, \{\delta_f, v\}) = \left[F_{A\delta}^{y,z}(x, y, \{\delta_f, v\}) \quad M_{A\delta}(x, y, \{\delta_f, v\}\right]^T \tag{24}$$

where: $F_{A\delta}^{y,z}$- is a two-component vector of aerodynamic force produced by the input control signal that contains only the components in the *y* and *z* axes.

The use of nonlinear equations in variant 3 significantly affected the efficiency of the algorithm. The time of a single process was extended so much that it was impossible to use it in real-time applications [37], [38], [39], [40].

In order to shorten the computation time, the scope of the algorithm has been limited by omitting the "z" component of the aerodynamic force from the input control signal from the equation of constraints.

It was assumed that changes in the "z" axis can be easily compensated by changes in the angle of attack of the aircraft.

In this way, another reconfiguration algorithm was created (variant 4), which can be expressed as follows:

$$\min_{\delta_f} f_{\delta_f} \; dla \; \{f_{A\delta}(x,y,\delta_f,\upsilon) - f_{A\delta}(x,y,\delta) = 0\} \quad (25)$$

where:

$$f_{A\delta}(x,y,\delta) = \left[F^{y}_{A\delta}(x,y,\delta) \quad M_{A\delta}(x,y,\delta\right]^{T} \quad (26)$$

$$\mathrm{f_{A\delta}(x,y,\{\delta_f,\upsilon\})} = \left[\mathrm{F^{y}_{A\delta}(x,y,\{\delta_f,\upsilon\})} \quad \mathrm{M_{A\delta}(x,y,\{\delta_f,\upsilon\}}\right]^{\mathrm{T}} \quad (27)$$

where: $F^{y}_{A\delta}$- is a side component of the aerodynamic force vector from the input control signal.

3 Simulation tests of algorithms reconfiguration of unmanned aircraft control system

The variants of the reconfiguration algorithm described above were tested using flight simulation of a maintenance-free aircraft model. The tests were aimed at checking the quality of the reconfiguration for each of the methods described.

In order to assess the quality of the reconfiguration, a criterion was adopted, including the comparison of the behavior of a fully functional and inoperative aircraft after reconfiguration, performing the flight in the same conditions and with the same configuration of faults and control signals.

It was assumed that the reconfiguration is fully positive if the change of the position of the damaged aircraft following reconfiguration is close to zero or if it is the same as in the fully functional plane.

The greater the difference between the location of the failure-free and damaged planes, the lower the efficiency of the given reconfiguration algorithm.

It should be noted that during the conducted tests, no differences in the variability of other state parameters were analyzed, as it was assumed that the change in the spatial orientation of the aircraft reflects well enough the ability to control the aircraft.

Aircraft are usually controlled by changing their characteristics, and changes in their flight path result from a change in the spatial position.

Flight speed control is an exception to this rule, it depends mainly on the thrust force generated by the propulsion unit.

Accordingly, for this state variable, it has been assumed that the aircraft propulsion unit is operational and that it produces enough thrust to achieve a predetermined flight speed, it being noted that a reconfiguration algorithm is not required to provide the same controllability to a damaged ship as in a fully operational aircraft.

In the case of complex failures (including several failures at the same time), such a specificity of the reconfiguration system may prevent its functioning.

The advantage of reconfiguring the control system is the ability to improve the controllability of the aircraft to the extent that the control system design allows it, the nature of the failure and the effectiveness of the reconfiguration method.

During the tests, various fault and control signal configurations were simulated.

Next, a comparison was made between the change of position (orientation) of fully functional and damaged aircraft in relation to each developed variant of the reconfiguration algorithm.

The following damage configurations were assumed for the needs of the tests:

A. Lock the right aileron in the 5 degrees inclined position.
B. Locking the left rudder in the 5 degrees inclined position.
C. Steering rudder blocked in 3 degrees inclined position.
D. Simultaneous blocking of the right aileron (inclined by 5 degrees) and left rudder (deviation of 5 degrees).
E. Simultaneous blocking of the right aileron (deviation by 5 degrees) and rudder (deviation by 3 degrees).
F. Simultaneous locking of the left rudder (deviation by 5 degrees) and rudder (deviation by 3 degrees).

In turn, the configurations of the input control signals *(δ)* simulated during the tests were as follows:

1. A double rectangular pulse signal (Figure 4) for tilt (ailerons).
2. Multiple rectangular pulse signal ("3-2-1-1") (Fig. 4) for inclination (elevator).
3. A double rectangular pulse signal (Fig. 4) for the deviation (rudder).
4. Parallel duplicate signals for tilt (aileron) and "3-2-1-1" for tilt (elevator).

5. Parallel double signals for tilt (aileron) and doubled signal for deflection (rudder).
6. Parallel duplicate signals for deviation and "3-2-1-1" for inclination.
7. Parallel duplicate signals for tilt and yaw and "3-2-1-1-1" for tilt.

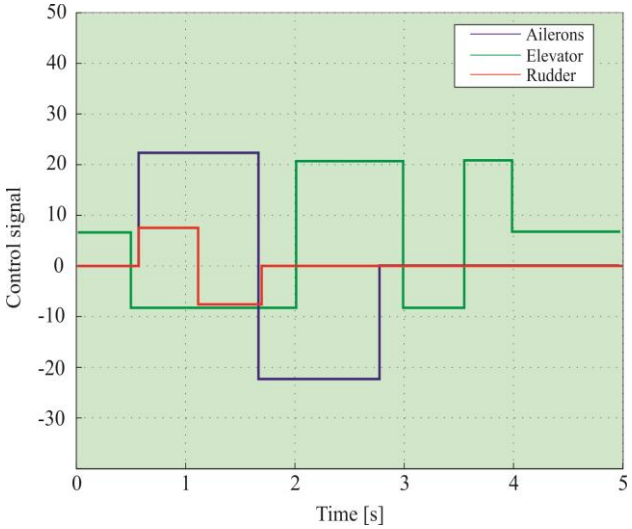

Fig. 4 Waveform of input control signals δ expressed as a percentage of their maximum values

The shapes of the input signals of the control signals correspond to the signals of standard signals used in the research of dynamic properties and in the identification of the aircraft's flight dynamics. These signals are easy to implement and trigger a predictable response by the aircraft to a control signal [41], [42], [43], [44].

During the tests, simulations of all damage combinations (A to F) and all control signals (1 to 7) were performed. Then the courses of changes of the position of the inoperative aircraft without reconfiguration and after reconfiguration (for all variants of the reconfiguration algorithm) were compared with the charts of the position of the functional aircraft for the same input control signals.

For comparison, an integrated square quality indicator is used in the following form [45]:

$$I_R = \int_0^{tk} (x_{bawarii} - x_{zawaria})^2 dt \qquad (28)$$

where: *x*- is the compared signal, and t_k- the time of the end of the simulation.

The smaller the difference between the response of a failure-free object and a defective one, the lower the value of the quality indicator. The obtained results of the comparison between the efficient aircraft and the disabled were subjected to statistical analysis in order to determine the average value and distribution of the quality index for all combinations of failures and control signals (a total of 42 cases).

In order to facilitate the analysis of such significant amounts of data, the results have been grouped into three categories:

I. Single fault (A-C) and single control signal (1-3).
II. Double failure (A-F) and single control signal (1-3).
III. Single fault (A-C) and two or three control signals (4-7).

The arithmetic mean and standard deviation values of the quality index for the first category of results are shown in Table 1, where the mean and standard deviation values for the unpaired aircraft without reconfiguration are much higher than after reconfiguration, and the differences between mean values for all variants of the reconfiguration algorithm are not high.

The best reconfiguration quality was obtained for the third variant and fourth, however, it can not be unambiguously determined which of the two options is the best.

Table 1. Quality indicator statistics for the first category of results

	Arithmetic average	Standard deviation
No configuration	1,544.78	2,006.62
Variant 1	65.77	142.05
Variant 2	60.74	143.92
Variant 3	45.45	104.15
Variant 4	41.59	127.32

In the fourth variant, the lowest mean value was obtained, while in the third variant the average is slightly higher, but the distribution is narrower.

In turn, detailed analyzes of statistical data showed that all algorithm variants were the most struggling with the reconfiguration of aileron faults. For this type of failure, the highest values of the quality indicator were obtained.

This is due to the fact that the failure of the aileron generates a significant deflection moment which can be compensated only by the rudder. The deflection of the rudder, however, creates an additional heeling moment and lateral force, which is difficult to compensate, because the additional control surfaces can produce lateral forces significantly lower than the force generated by the rudder. The next drawings (Figures 19-21) show exemplary graphs of changes in the angle of the aircraft's failure-free and defective position, with or without reconfiguration, in case of failure of the elevator (B failure) and signal for inclination of "3-2-1-1" (signal 2).

It can be clearly seen that a damaged plane without reconfiguration is not able to achieve a specific change in tilt. In addition, the tilting and deviation of the aircraft is constantly increasing.

Analyzes of all simulations showed that positioning errors without reconfiguration can reach up to 70 degrees. In the second result category, option 4 of the reconfiguration algorithm (Table 2) is the most effective. Other algorithms dealt with the problem a bit better than a non-reconfigurable system. It is clear that options 2 and 3 were worse than in the case of no reconfiguration.

Table 2. Quality indicator statistics for the second category of results

	Arithmetic average	Standard deviation
No configuration	3,621.31	3,922.85
Variant 1	3.362.81	8,749.31
Variant 2	5,952.84	11,469.72
Variant 3	4,424.47	7,711.13
Variant 4	852.78	1,797.82

A parallel failure of the elevator and rudder (F failure) turned out to be the most difficult to reconfigure for all variants of the algorithm.

In most cases of this configuration, the aircraft lost controllability, which in combination with locked, tilted control surfaces caused uncontrolled rotation in the tilt and yaw channels.

The high values of the quality indicator for this combination of damage depend mainly on the time after which the aircraft lost control.

As detailed analysis has shown, the use of some variants of the algorithm has destabilized the flight path of the aircraft earlier than in the absence of reconfiguration.

In the case of other failure configurations, all variants of the reconfiguration algorithm allowed to obtain a better quality indicator than in the case of a lack of reconfiguration.

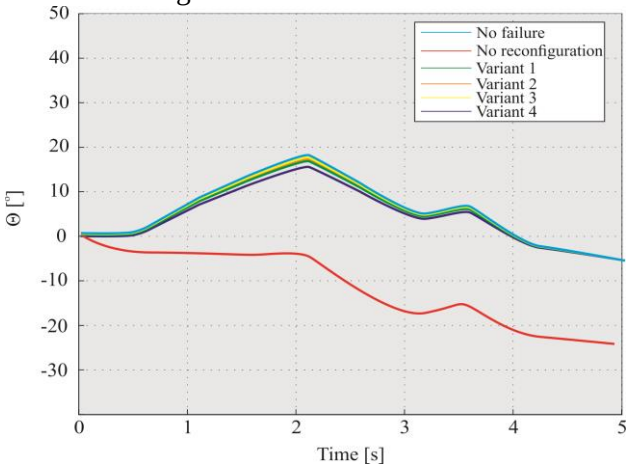

Fig. 5 Changes in the angle of inclination for the first category of results

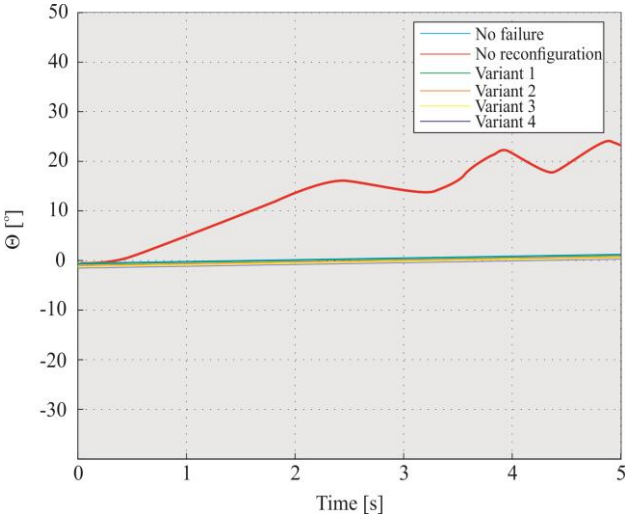

Fig. 6 Changes in the tilt angle for the first category of results

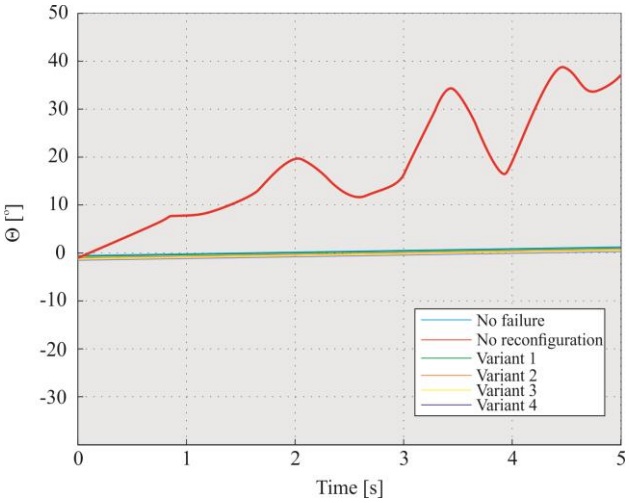

Fig. 7 Changes in the angle of inclination for the second category of results

4 Conclusions

The performed simulations of various fault and control signal configurations have shown that the proposed reconfiguration method allows compensation of the causes of the control system failure. The control signals produced by the reconfiguration system were within the permissible range of deflections for individual control surfaces.

In the case of individual failures, the most difficult to reconfigure was the aileron failure due to the generated deflection moment and the inability to generate, by the remaining surfaces, sufficient forces to compensate for this moment. However, it should be noted that despite the fact that in the event of such failure, the quality indicators are the least favorable, after the reconfiguration the aircraft is under full control. The situation is much worse in the case of reconfiguration with double damage.

In most cases, the quality indicators are much higher and the behavior of the aircraft after reconfiguration differs noticeably from the behavior of a failure-free aircraft.

In turn, in the event of simultaneous failure of the elevator and rudder, the aircraft loses the ability to control and control both in the case of unconfiguration, as well as in the case of the majority of variants of reconfiguration algorithms.

References:

[1] W. R. Donovan, *The Design of an Uninhabited Air Vehicle for Remote Sensing in the Cryosphere*, Master's Thesis, Department of Aerospace Engineering, The University of Kansas, Lawrence, KS, 2007.

[2] S. Underwood, *Performance and Emission Characteristics of an Aircraft Turbo diesel Engine using JET-A Fuel*, Master's Thesis, Department of Aerospace Engineering, The University of Kansas, Lawrence, KS, 2008.

[3] R. Burns, *A Low-Cost Modular- Avionics and telemetry Software System for the CReSIS Meridian Uninhabited Aerial System*, 27th Digital Avionics Systems Conference, St. Paul, MN, 2008.

[4] T. Samad, J.S. Bay, D. Godbole, *Network-centric systems for military operations in urban terrain: The role of UAVs*, Proceeding of the IEEE, 95, pp. 92-107, 2007.

[5] R. Jager, *Test and Evaluation of the Piccolo II Autopilot System on a One-Third Scale Yak-54*, Master's Thesis, Department of Aerospace Engineering, The University of Kansas, Lawrence, KS, 2005.

[6] J. Esposito, *Time Plotting Framework for Remote Display of Flight Dat*a, 27th Digital Avionics Systems Conference, St. Paul, MN, 2008.

[7] L. Setlak and R. Kowalik, *Studies of 4-rotor unmanned aerial vehicle UAV in the field of control system*, 22nd International Conference on Circuits, Systems, Communications and Computers (CSCC 2018), MATEC Web of Conferences, Vol. 210, pp. 1-9, 2018.

[8] H. I. Leong, *Modeling and Simulation for the Yak-54 using a 6DOF Model with Flight Test Validation*, Technical Report, Center for Remote Sensing of Ice Sheets, The University of Kansas, Lawrence, KS, 2008.

[9] M. Z. Babar, *Robust Integrated Lateral Guidance and Control of UAVs*, Master's Thesis, Electrical Engineering Department, Muhammad Ali Jinnah University, Islamabad, Pakistan, 2013.

[10] M.V. Cook, *Flight Dynamics Principles*, Elsevier Butterworth-Heinemann, 1997.

[11] J. Roskam, *Aircraft Flight Dynamics and Automatic Flight Controls (Part I)*, DAR Corporation, Lawrence, KS, 2003.

[12] H-M. Huang, *Autonomy Levels for Unmanned Systems Framework*, Volume I: Terminology, Version 1.1, NIST Special Publication: Gaithersburg, MD, USA, p. 1011, 2004.

[13] H-M. Huang, K. Pavek, M. Ragon, Jones, E. Messina, J. Albus, *Characterizing Unmanned System Autonomy: Contextual Autonomous Capability and Level of Autonomy Analyses*. In Unmanned Systems Technology IX, 2007, International Society for Optics and Photonics: San Diego, CA, USA, p. 65611N, 2007.

[14] A. Ollero, L. Merino, *Control and perception techniques for aerial robotics*, Annual Reviews in Control, 28, pp. 167-178, 2004.

[15] S. Dufresne, C. Johnson, D. N. Mavris, *Variable fidelity conceptual design environment for revolutionary unmanned aerial vehicles*, Journal of Aircraft, 45, 1405-1418, 2008.

[16] B. Friedland, *Control System Design, Manager, Systems Research Kearfott Division*, The Singer Company and Polytechnic Institute of New York, 2013.

[17] R. Kozma, W. J. Freeman, *Basic principles of the KIV model and its application to the navigation problem*, Journal of Integrative Neuroscience, 2, pp. 125-145, 2003.

[18] T.R. Browning, *Applying the design structure matrix to system decomposition and integration problems: A review and new directions*, IEEE Trans. Eng. Manag., 48, pp. 292-306, 2001. [CrossRef]

[19] P. Verschure, T. Voegtlin, R.J. Douglas, *Environmentally mediated synergy between perception and behavior in mobile robots*. Nature, 425, pp. 620-624, 2003.

[20] D. Harter, R. Kozma, *Chaotic neurodynamics for autonomous agents*, IEEE Transactions on Neural Networks, 16, pp. 565-579, 2005.

[21] J. D. Galloway, *Optimization of Conceptual Aircraft Design for Stability/Control and Performance*, Master's Thesis, Department of Aeronautics and Astronautics, University of Washington, 2000.

[22] K. Valavanis, R. Oh, L.A. Piegl, *Unmanned Aircraft Systems: International Symposium on Unmanned Aerial Vehicles*, UAV'08; Springer

Science & Business Media: New York, NY, USA, 2008.

[23] C. Eaton, E. Chong, A. Maciejewski, *Multiple-scenario unmanned aerial system control: A systems engineering approach and review of existing control methods*. Aerospace 2016, 3,1. [CrossRef]

[24] Lucjan Setlak, Rafał Kowalik, Wojciech Redo, *Technological Solutions of Selected Components of Energo-electronic Power Supply System PES in the Field of AC/DC/DC*, Processing in Accordance with a Trend of More Electric Aircraft, International Journal of Circuits, Systems and Signal Processing, ISSN: 1998-4464, Volume 11, 2017.

[25] H. González-Jorge, J. Martínez-Sánchez, M. Bueno, R. Arias, *Unmanned aerial systems for civil applications: A review*, Drones 2017, 1, 2. [CrossRef]

[26] F. Kendoul, *Towards a unified framework for UAS autonomy and technology readiness assessment (ATRA)*, In Autonomous Control Systems and Vehicles: Intelligent Unmanned Systems, 2015.

[27] K. Nonami, M. Kartidjo, Yoon, K.-J. A. Budiyono, Eds., Springer: Tokyo, Japan, pp. 55-71, 2013.

[28] Y. Bae J Kim., Y. Kim *Obstacle avoidance methods in the chaotic mobile robot with integrated some chaos equation*, International Journal of Fuzzy Logic and Intelligent Systems, 3, pp. 206-214, 2003.

[29] Lucjan Setlak, Rafał Kowalik, *Stability Evaluation of the Flight Trajectory of Unmanned Aerial Vehicle in the Presence of Strong Wind*, WSEAS Transactions on Systems and Control, ISSN/E-ISSN: 1991-8763/2224-2856, Volume 14, , Art. #6, pp. 43-50, 2019.

[30] P. Arena, S. De Fiore, L. Fortuna, L. Patané, *Perception-action map learning in controlled multiscroll systems applied to robot navigation*, Chaos: An Interdisciplinary Journal of Nonlinear Science, 18, pp. 1-16, 2008.

[31] R. Collopy, C.L. Bloebaum, B.L. Mesmer, *The distinct and interrelated roles of value-driven design, multidisciplinary design optimization, and decision analysis*. In Proceedings of the 14th AIAA/ISSMO Multidisciplinary Analysis and Optimization Conference, Indianapolis, IN, USA, 17-19 September 2012.

[32] D. Norris, *Build Your Own Quadcopter: Power up Your Designs with the Parallax Elev-8*, McGraw Hill Professional: New York, NY, USA, 2014.

[33] M. Carrascosa, S.D. Eppinger, D.E. Whitney, *Using the design structure matrix to estimate product development time*. In Proceedings of the ASME Design Engineering Technical Conferences (Design Automation Conference), Atlanta, GA, USA, 13-16 September 1998; pp. 1-10, 1998.

[34] A. Yassine, *An introduction to modeling and analyzing complex product development processes using the design structure matrix (DSM) method*, Urbana, 52, pp. 1-17, 2004.

[35] G.V. Bhatia, C. Wenger, N.S. Basha, T.R Subramanian, S. Shihab, *AERE 568X Final Project: A Comparison of the Traditional Systems Engineering Approach with Value-Driven Design and Incorporation of Uncertainties-An Aircraft System Case Study*; MIT: Cambridge, MA, USA, 2015.

[36] R. Siegwart, I.R. Nourbakhsh, D. Scaramuzza, *Introduction to Autonomous Mobile Robot*, MIT: Cambridge, MA, USA, 2011.

[37] P. Verschure, P. Althaus, *A real-world rational agent: Unifying old and new AL Cognitive Science*, 2003, 27, pp. 561-590. Freeman W J. Simulation of chaotic EEG patterns with a dynamic model of the olfactory system. Biological Cybernetics, 56, pp. 139-150, 1987.

[38] X. Li, G. Li, L. Wang, W. J. Freeman, *Study of a bionic pattern classifier based on olfactory neural system*, Journal of Bionic Engineering, 1, pp. 133-140, 2004.

[39] W. J. Freeman, *How and why brains create meaning from sensory information*, International Journal of Bifurcation and Chaos, 14, pp. 515-530, 2004.

[40] W. J. Freeman *A neurobiological theory of meaning in perception. Part I: Information and* meaning in nonconvergent and nonlocal brain dynamics, International Journal of Bifurcation and Chaos, 13, pp. 2493-2511, 2003.

[41] W. J. Freeman *The physiology of perception*, Scientific American, 264, pp. 78-85, 1991.

[42] M. E. Yalcin, J. A. K. Suykens, J. Vandewalle *True random bit generation from a double scroll attractor*, IEEE Transactions on Circuits and Systems I: Regular Papers, 51, pp. 1395-1404, 2004.

[43] R. Kozma, W. J. Freeman, *The KIV model of intentional dynamics and decision making*, Neural Networks, 22, pp. 277-285, 2008.

[44] Lucjan Setlak, Rafał Kowalik, Wojciech Redo, *Study of Multi-Pulse Rectifiers of the PES System in Accordance with the Concept of a More Electric Aircraft*, WSEAS Transactions

on Systems and Control, ISSN/E-ISSN: 1991-8763/2224-2856, Volume 13, Art. #20, pp. 161-170, 2018.

[45] J. Lu, G. Chen, X. Yu, H. Leung, *Design and analysis of multiscroll chaotic attractors from saturated function series*, IEEE Transactions on Circuits and Systems I: Regular Papers, 51, pp. 2476-2490, 2004.